ENGINEERING TRANSACTIONS • *Engng. Trans.* • **42**, 4, 399–416, 1994
Polish Academy of Sciences • Institute of Fundamental Technological Research

ON A CERTAIN THEORY OF PLASTICITY SOLUTIONS FOR THE HEAVY MACHINE EARTH-WORKING PROCESS

A. JARZĘBOWSKI, D. SZYBA
and W. TRĄMPCZYŃSKI (WARSZAWA)

The aim of this paper is to apply kinematic solutions of the theory of plasticity for description of a soil shoving process for such heavy machine tools as buckets of the loading machines, excavators etc. Assuming the material to be rigid-plastic with softening, which obeys the Coulomb–Mohr yield criterion and the associated flow rule, kinematic solutions for the initial and subsequent phases of the process were found. Characteristic rigid zones, which are periodically generated during the cohesive soil cutting process, and periodicity of the resulting force were predicted in this way. Then, theoretical results were compared with experimental data showing good agreement with theoretical prediction.

1. Introduction

The earth-moving process realized by heavy machines is energetically very ineffective and its proper theoretical description can be of important engineering significance. It can result in obtaining optimal shoving trajectories and considerable energy savings. In this paper, a model based on the mathematical theory of plasticity is applied to describe initial and more advanced stages of the shoving process. The process is considered as the problem of passive pressure exerted by a cohesive granular material on a rigid wall shaped similarly to the heavy machine tools.

The problem of passive and active pressures exerted by a granular medium on a rigid wall under plane strain conditions has quite a broad literature. Several theoretical solutions (for statics, as well as for kinematics) were found within the theory of plasticity, under the assumption of a rigid-perfectly plastic behaviour of granular material, using the method of characteristics [1–6].

Although a great number of boundary value problems, for incipient tools motion, were solved in this way, several limitations in obtaining complete

or only kinematically admissible solutions, were found [7]. It was found very difficult to analyse more advanced stages of such processes using this technique (as, for example, the process of moving walls in a way similar to that for heavy machine tools).

Hence, a simplified technique, based on kinematically admissible mechanisms for a Coulomb-Mohr material [8] and a Coulomb-Mohr material with softening [9-11] was proposed to analyse the mechanics of the heavy machine tool filling process.

The method of kinematically admissible mechanisms was used also by MICHALOWSKI [12] to describe periodicity of the processes of flow from hoppers. A model of a non-cohesive, granular material with strain-softening was incorporated in that paper. An assumption was made that a change of material parameters across the slip-line (shear band) occurred, which resulted in quite satisfactory coincidence with the experimentally observed flow patterns.

In the case of kinematically admissible solutions, an infinite number of solutions can be constructed for any particular problem. Then the kinematics related to minimum force exerted on the tool is analyzed. Investigation of such solutions depends very much on personal experience and have to be supported by an extensive experimental program. Such a program, for cohesive soil (for two different values of cohesion) and four different types of heavy machine tools, was performed under the plane strain conditions and presented in [13]. The initial stage of the shoving process was observed and detected using a special experimental stand with transparent walls. The comparison of theoretical and experimental results shows that the incipient stage of the shoving process can be described by means of simple kinematically admissible solutions, assuming the Coulomb-Mohr material and the associated flow rule.

Results of an experimental program, carried out by the present authors, for more advanced stages of the shoving process shows that two types of kinematic schemes of the process can be distinguished. The first one, similar to that presented in [10] and the second one, suggested by Z. MRÓZ [14], will be discussed in this paper. Similar kinematic mechanisms were also observed in [13]. Theoretical solutions, based on those two schemes, are proposed in this paper by assuming a Coulomb-Mohr material with softening and the associated flow rule. Those solutions are then compared with experimental results showing a fairly good coincidence.

It should be also emphasized that, as for today, there is no other simple method to follow such complicated processes as those considered herein.

2. Kinematically admissible solutions for wall pressure problems

According to the limit load theorems for rigid-perfectly plastic materials and the associated flow rule, any statically admissible solution defines a lower bound of the limit load, and each kinematically admissible solution defines an upper bound. Hence, if it is not possible to find a complete solution to a particular problem, one may attempt to find a certain upper and a lower bounds on the limit load. If the difference between those two solutions is not too large, a reasonable estimate of the unknown complete solution may be arrived at.

If strain-hardening (softening) is accounted for, the kinematic solution does not provide an upper bound since the limit load theorems can not be proved. In fact, selection of the kinematic field in a hardening/softening material is equivalent to the selection of a spatial distribution of perfectly plastic materials with different yield conditions. Since the distribution of inhomogeneities resulting from the kinematic solution may differ from the true solution, no rigorous bound to the true load can be established. Thus, load evaluation for hardening materials which is based on the kinematic method may only be regarded as an engineering approach.

Let us consider the soil displacement which is due to the motion of the L-shaped rigid wall (of height H), which moves horizontally with velocity v_0 pushing the soil which has a horizontal free boundary BD (Fig. 1). It is assumed that the wall is wide enough to consider the process to run under plane strain condition.

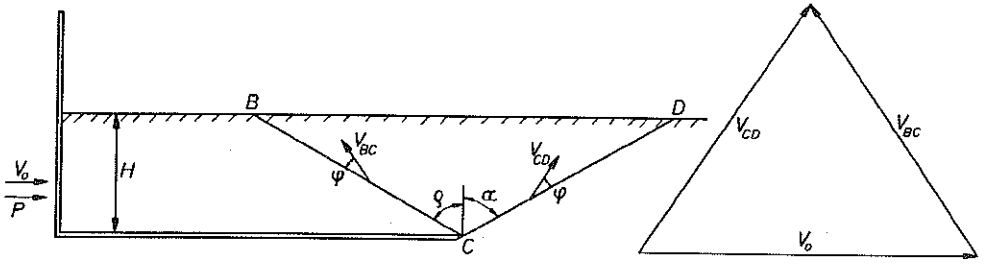

FIG. 1. Rigid wall (shaped similarly to the loading machine bucket) pressure problem, and its kinematically admissible solution.

Assuming the material to be rigid-perfectly plastic and to obey the Coulomb–Mohr yield criterion

$$f = (\sigma_1 - \sigma_2) - (\sigma_1 + \sigma_2 + 2H)\sin\varphi = 0, \tag{1}$$

where $H = c\,\mathrm{tg}^{-1}\varphi$, c – material cohesion and φ – internal friction angle,

the associated flow rule takes the form:

$$\dot{\varepsilon}_{ij} = \lambda \frac{\partial f(\sigma_{ij})}{\partial \sigma_{ij}}. \tag{2}$$

In several papers [15, 16] it was shown that the associated flow rule for the Coulomb-Mohr material was not a good approximation of real material behaviour. Basically it concerns the dilatation effect, which is overestimated in such a case. The experiments supporting such a conclusion were performed mainly on a material without cohesion – dry sand.

As it was mentioned before, results of the extensive experimental program performed using a special material with cohesion [13], show the applicability of the associated flow rule and Coulomb-Mohr yield criterion, at least for the incipient motion. It is manifested as a good correlation between the experimental and theoretical slip mechanisms and slip lines inclination. Dilatation along the slip lines (for incipient motion) also reveals visible cracks with an obvious volume increase. Similar results, for the same material, were obtained also in this paper by the present authors, who observed applicability of the associated flow rule also for a more advanced stage of the process, at least within the accuracy limited by the assumption of rigid-plastic behaviour of the material.

3. Soil shoving process by a rigid wall

3.1. The incipient motion solution

A simple kinematically admissible mechanism (Fig. 1) may be assumed, which consists in the motion of the rigid triangle ΔBCD along the slip lines CD and BC. Such a mechanism is observed experimentally and was found to be (energetically) the most efficient solution among those previously considered by the authors [10].

The value of the force P, which is necessary to realize the incipient motion, can be determined from the following energy balance equation:

$$P \cdot V_0 = D_{cd} + D_{bc} + D_g, \tag{3}$$

where D_{cd} – energy dissipated along the slip-line CD, D_{bc} – energy dissipated along the slip-line BC, D_g – the increase of potential energy of the block ΔBCD (in the case when the material weight is accounted for).

The energy dissipation rate per unit length for the associated flow rule along the slip lines (such as CD and CB) is described by the following

equation [8]:

$$D_l = c \cdot \cos\varphi \cdot V_l, \tag{4}$$

where V_l – denotes the velocity jump along the slip line.

Since the material is assumed to be weightless, we have $D_g = 0$.

3.2. The effects on the velocity discontinuity line

In plasticity of granular media, the velocity discontinuity line is usually interpreted as a finite thin layer (b_0), across which the velocity changes rapidly (Fig. 2). Moving from zone *1* (particle velocity V_1) to zone *2* (particle velocity V_2), the material undergoes a velocity "jump", ΔV, which is inclined at an angle φ (when the Coulomb-Mohr material and the associated flow rule are assumed) to the discontinuity line (CD).

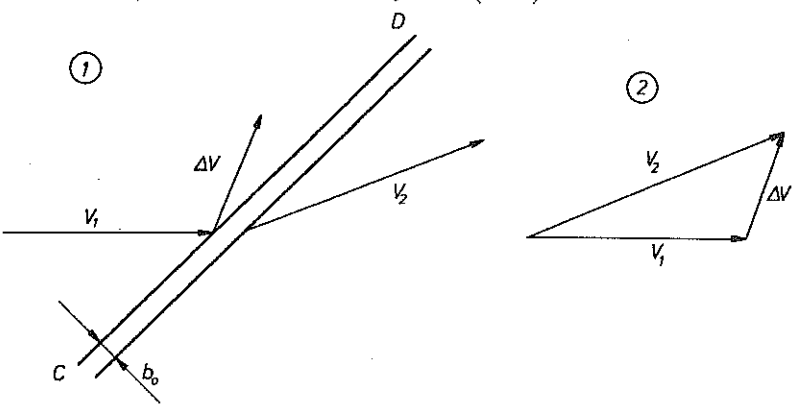

FIG. 2. Discontinuity line velocity relations.

In this paper, the approach assuming the motion of a slip line of zero thickness within the material was adopted.

Let us assume that slip line CD, inclined at an angle α, penetrates the virgin material layer of thickness H with constant horizontal velocity V_0 (Fig. 3a). When the line moves, the material on the line undergoes velocity jump ΔV, inclined at an angle φ to the slip-line (associated flow rule and Coulomb-Mohr material). This jump can be separated into the shear (ΔV_t) and normal (ΔV_n) components. As a result, the material left behind the moving slip line is sheared and dilatated (consolidation of the new material is not considered). It is assumed that this processes (shear and dilatation) can change material properties in the way described by two parameters explained below.

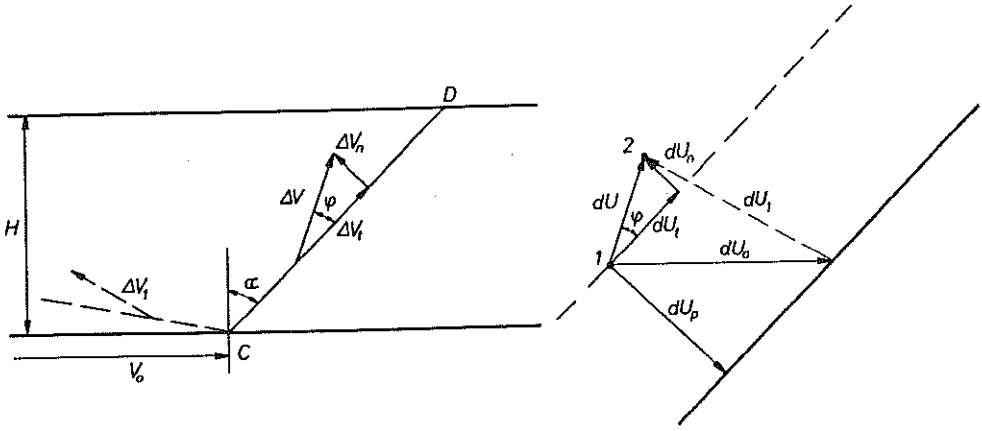

FIG. 3. Velocity and displacement components on the discontinuity line.

Let us discuss a small slip-line displacement (step) dU_0 (Fig. 3b). As a result of velocity jump ΔV, material point 1 moves to a new position 2 (as a result of shear and dilatation process), and this displacement can be decomposed into tangential (dU_t) and normal (dU_n) components, which illustrate respectively the material shear and dilatation. In order to describe the influence of these two effects on the material behaviour, two different parameters were introduced:

- for dilatancy – the parameter U_{n_i}:

$$U_{n_i} = dU_{n_i}/dU_{p_i}; \tag{5}$$

- for shear – the parameter U_s:

$$\begin{aligned} U_s &= \sum_{i=1}^{k} U_{s_i}, \\ U_{s_i} &= dU_{t_i}/dU_{p_i}, \end{aligned} \tag{6}$$

where dU_{n_i} and dU_{s_i} are defined according to the corresponding normal and tangential components of the displacement changes for the particle within a single subsequent step i, and dU_{p_i} is a normal component of the displacement of the discontinuity line (Fig. 3b), and k denotes the number of consecutive slip lines passing through the material zone under consideration. It means that, in the case when through a certain area a discontinuity line passes several times, the material behaviour influenced by shear is described by the parameter, which is the sum of subsequent steps.

The first parameter influences only the material density:

$$\gamma_i = \frac{\gamma_{i-1}}{U_{n_i} + 1}, \tag{7}$$

where γ_{i-1} denotes the density of the material before the actual slip line passing.

It was assumed that the second parameter (describing material shear) influences only the material cohesion c (in the Coulomb-Mohr yield criterion) according to the following relation [17]:

$$c = (c_0 - c_R)\exp(-U_s \cdot A) + c_R, \tag{8}$$

where c_0 – cohesion of the virgin material, c_R – the residual cohesion value, A – a material constant. The dependence of cohesion c versus parameter U_s is depicted in Fig. 4 (for $c_0 = 19.6\,\mathrm{kPa}$, $c_R = 3.92\,\mathrm{kPa}$, $A = 0.8$).

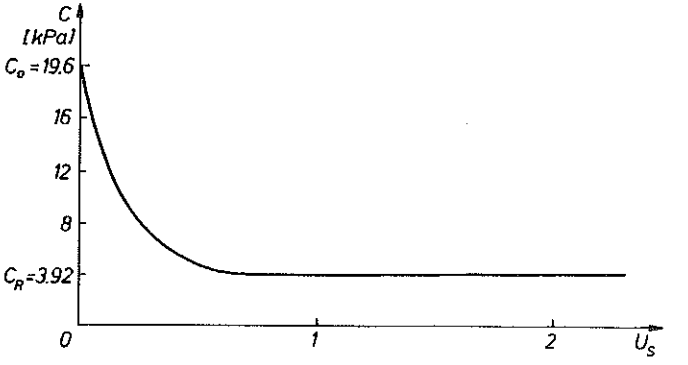

FIG. 4. Dependence of cohesion c versus parameter U_s.

3.3. The initial stage of soil shoving

As it was mentioned above, the incipient tool motion, in the case shown in Fig. 1, can be described by a simple solution, which consists of the motion of the rigid triangle ΔBCD along the slip lines CD and BC. Two different mechanisms, based on experimental observation, were then adapted to describe the subsequent shoving process. In the first one, discussed in [10], two slip lines are assumed (Fig. 1) and in the second one, three slip lines are assumed (Fig. 8). In both cases the solution is done in a step-by-step technique. The inclination and position of the consequent slip lines are calculated for the minimum moving forces, taking into account material parameters (shear and dilatation) which result from the previous step of the process.

3.3.1. Two slip line solutions. Let us consider several subsequent steps of the cutting process (Fig. 1), all with constant lateral displacement U_0.

Some of the following phases are shown in Figs. 5–7. It was found that the mechanism shown in Fig. 1, consisting of the rigid triangle motion was, in terms of the energy, the most effective mechanism during the entire process considered. The presented solution is a modified version of that shown in [10], and will be discussed shortly.

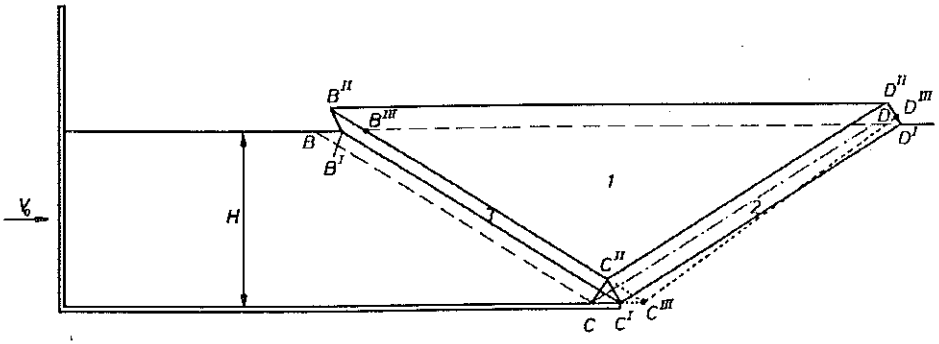

FIG. 5. Kinematically admissible solution at a particular stage of the rigid wall cutting process (the first and the second steps).

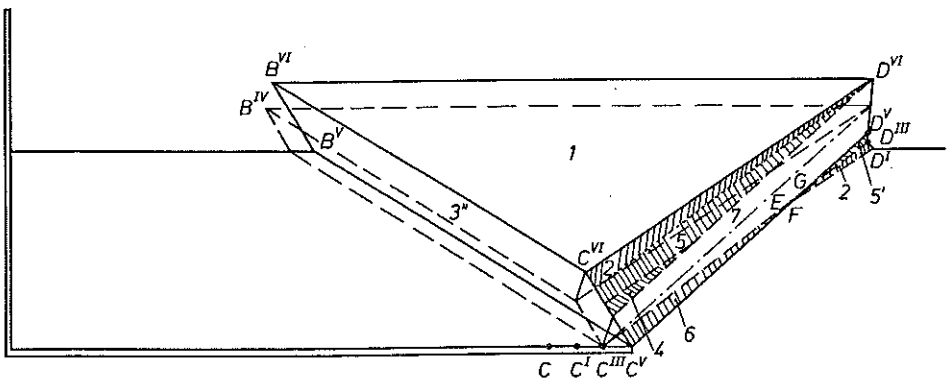

FIG. 6. Kinematically admissible solution at a particular stage of the rigid wall cutting process.

As it was mentioned before, the solution was carried out in a step-by-step way. In every step, the new, energetically most effective (Eq. (3)) positions of the slip lines (values of the angles α and ρ – see Fig. 1) were calculated, assuming a new position of the tool (after displacement), but taking into account material parameters resulting from the previous step. Then, a proper hodograph was built and the material displacement were calculated.

Such a solution, for the first and the second steps, is shown in Fig. 5, where kinematic mechanism for incipient motion (motion of the rigid triangle ΔBCD along the slip lines CD and BC) is marked by a solid line.

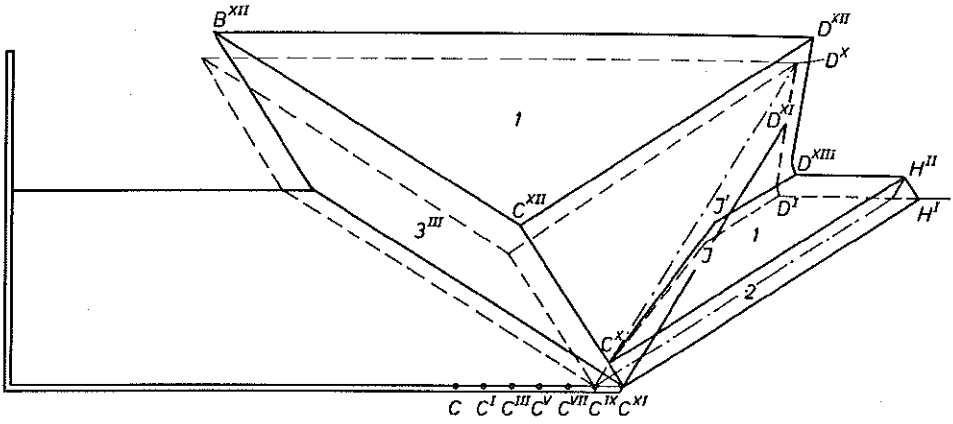

FIG. 7. Kinematically admissible solution at a particular stage of the rigid wall cutting process (advanced tool displacement).

The new position of the tool C^{I} (after the first lateral displacement U_0) was assumed, and new optimal positions of slip lines ($C^{\mathrm{I}}D^{\mathrm{I}}$ and $C^{\mathrm{I}}B^{\mathrm{I}}$) were calculated. Because in a former step, the material was a virgin one, position of the slip lines are the same as that for incipient motion. Having the new slip line positions ($C^{\mathrm{I}}D^{\mathrm{I}}$ and $C^{\mathrm{I}}B^{\mathrm{I}}$), the hodograph was built and material displacement (as a result of lateral displacement U_0) was calculated. Taking into account the changes of material parameters, changes due to shear and dilatation as the slip lines moves (Eqs. (5) and (6)), zones of different material parameters can be distinguished: *1* – virgin material, *2* – shear and dilatated zone, *3* – shear and dilatated zone. Assuming the next step (Fig. 5 – position C^{III}), material parameters in the zones mentioned above has to be taken for calculation of new optimal slip lines ($C^{\mathrm{III}}D^{\mathrm{III}}$ and $C^{\mathrm{III}}B^{\mathrm{III}}$) positions (step 2). It appears that, because of new material parameters in zone 2, the optimal slip line position ($C^{\mathrm{III}}D^{\mathrm{III}}$) is no longer parallel to former one ($C^{\mathrm{I}}D^{\mathrm{I}}$) and changes its orientation into a more inclined position (Fig. 5 – points). Hence, taking into account the zones of different material parameters, the following steps were calculated (Figs. 5–7).

The direction of the slip line CD changes during the process (the value of α decreases), while the direction of the slip line BC remains constant (compare $C^{\mathrm{I}}D^{\mathrm{I}}$ and $C^{\mathrm{V}}D^{\mathrm{V}}$ lines and $B^{\mathrm{I}}C^{\mathrm{I}}$ and $B^{\mathrm{V}}C^{\mathrm{V}}$ lines in Figs. 5 and 6). The process produces different material zones with different values of material parameters, which results in their spatial distribution (for example, after the third step (Fig. 6) one can distinguish seven zones). This spatial distribution was taken into account while searching for optimal slip-line position after each step, and the dissipated energy (Eq. (3)) was calculated by taking into account the length of the slip lines within each zone.

The slip-line position after every step was marked by solid lines in each of the figures, while before the step it was marked by dashed lines.

The slip line CD changed its orientation into a more inclined, only to reach the step shown in Fig. 7, when the slip-line position $C^{XI}H^{I}$ turns out to be energetically more efficient than the position $C^{XI}D^{XI}$. From this moment on, the process proceeds similarly as that described above and develops periodically.

3.3.2. Three slip-lines solution. The basic concept of such a solution is shown in Fig. 8. It consists of a motion of the rigid triangle ΔBFD and the area CFG along the slip lines FD and FB, and CG and CF. Since the process is considered to be continuous, the area ΔCFG is not a rigid one, but consists of material dilatated and sheared as a result of a subsequent CG slip line forward movement. The triangle ΔBFD moves along the slip line FB slower than the area CFG along the line CF ($V_3 > V_1$). As a consequence, the last one penetrates the dilatated zone resulting from the slip line FD of the previous forward movement.

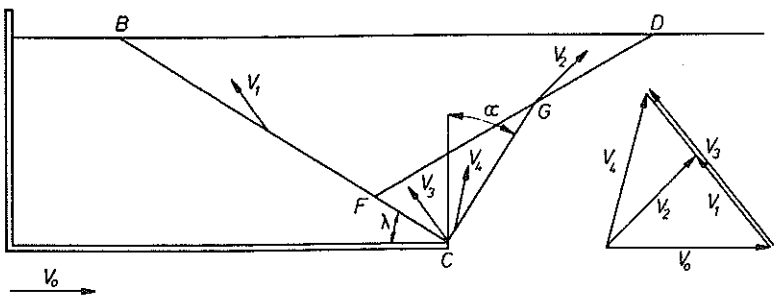

FIG. 8. Basic concept of the three slip-lines solution.

It was assumed that the mechanism mentioned above can be decomposed into two simple simultaneous processes:

- motion of the rigid triangle ΔBCD along the slip lines BC and CD;
- cutting the slope CD by the material edge BC (such a process is shown in Fig. 9, where the rigid triangle ΔBCD was removed, and the advanced stage of the process is presented).

Having assumed the three slip-lines mechanism (Fig. 8), let us consider several subsequent steps of the wall pressure process, all with constant lateral displacement U_0. The first step of the process has to be considered as a two slip-lines solution, as in Fig. 5. Then, the mechanism of stiff triangle ΔBFD motion along slip lines BF and FD and the mechanism of material sliding along slip line CG (slope cutting) are realized (Fig. 10). Some subsequent stages of such a process are presented in Figs. 10–11.

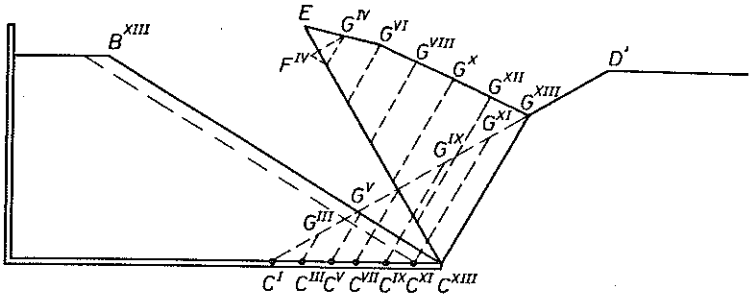

FIG. 9. Advanced stage of the rigid edge moving process.

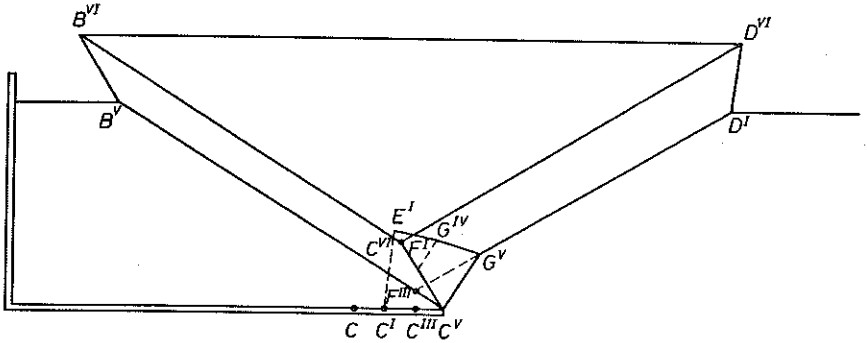

FIG. 10. A particular stage of the rigid wall cutting process – three slip-lines solution.

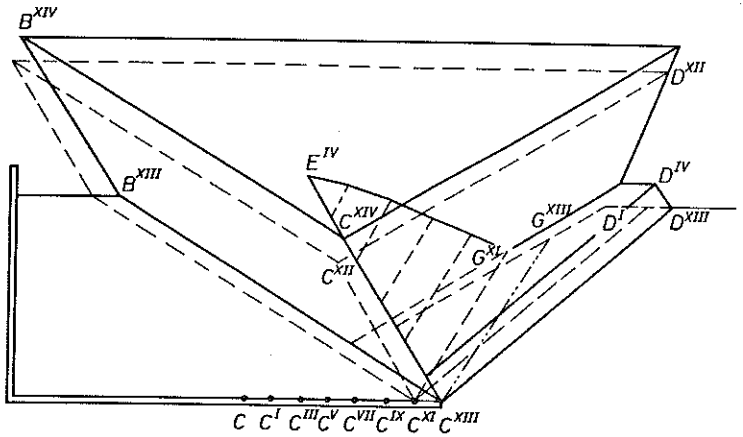

FIG. 11. Advanced stage of the rigid wall cutting process (the "jump" of the slip line).

The calculation technique was similar to that used for two slip-lines solution. As before, in every step, the new, energetically most effective (Eq. (3)) positions of the slip line CG (values of the angle α – see Fig. 8) were calculated assuming a new position of the tool (after displacement), and taking

into account the zones of different material parameters resulting from the previous step. Building the hodographs, the material displacement in every step was established and new zones containing material described by different parameters (as a result of material shearing and dilatation along the slip lines) were calculated.

The direction of the slip line CG was changing slightly in the process (the α value decreases), while the direction of the slip lines FB and FD (Fig. 10) remained constant.

The slip line CG moves until the step shown in Fig. 11, when the slip line position $C^{\mathrm{XIII}}D^{\mathrm{XIII}}$ turns out to be energetically more efficient than the position $C^{\mathrm{XIII}}G^{\mathrm{XIII}}$, and the slip line "jumps" to the new position. From this moment on, the process proceeds similarly to that described above and develops periodically.

As it was mentioned before, it has been assumed that the proposed mechanism can be decomposed into two simple processes: motion of the rigid triangle ΔBCD (along the slip lines BC and CD), and material sliding along the CG line (cutting the slope). The triangle ΔBCD moves along the slip line CB slower than the material which slips along CG. It has been assumed that this material (which is sheared and dilatated as CG slip line moves forward) freely penetrates and can be stored in dilatated zone $D^{\mathrm{I}}D^{\mathrm{IV}}F^{\mathrm{I}}F^{\mathrm{III}}$ (Fig. 11) resulting from the slip along the CD line.

Although the mechanism described above is kinematically inadmissible, it was considered to be experimentally observed.

3.3.3. Numerical results. Theoretical solutions were made for the weightless material characterized by the following parameters:

$$c_0 = 19.6\,\mathrm{kPa}, \qquad c_R = 3.92\,\mathrm{kPa}, \qquad A = 0.8,$$

corresponding to the material used in experiments. The total thickness of the layer was $H = 56\,\mathrm{mm}$ (Fig. 1).

The value of force P (which is necessary for implementation of the shoving process) as a function of the tool displacement (calculated at every step) is shown in Fig. 12 using x-marks in the case of two slip-lines solution, and using bold dots in the case of three lines solution. The magnitude of horizontal force P (2.08 kN), at which the slip line changes its position from $C^{\mathrm{XI}}D^{\mathrm{XI}}$ to $C^{\mathrm{XI}}H^{\mathrm{I}}$ (Fig. 7), and from $C^{\mathrm{XIII}}G^{\mathrm{XIII}}$ to $C^{\mathrm{XIII}}D^{\mathrm{XIII}}$ (Fig. 11) is depicted in Fig. 12 (dashed line). Point L corresponds to the slip line position $C^{\mathrm{XI}}H^{\mathrm{I}}$. Point M is shown for the next subsequent step of the process, after the change of the slip line position. When the next slip line occurs (CH), the value of force, which is necessary to continue the cutting process,

decreases. Point N corresponds to the slip-line position $C^{XIII}D^{XIII}$ for the three slip-lines mechanism (Fig. 11).

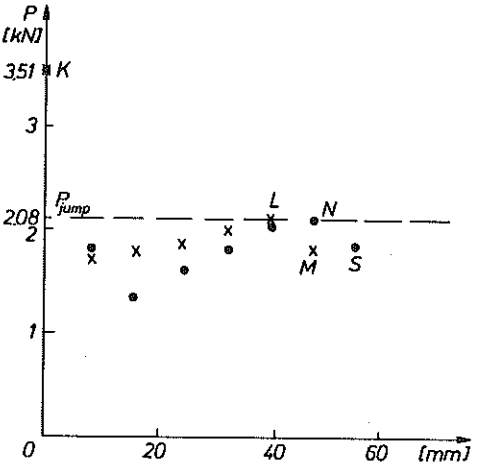

FIG. 12. Calculated values of the cutting force P (calculated for unit width of the tool) against the tool movement, • – the three slip-lines solution, × the two slip-lines solution.

4. EXPERIMENTAL RESULTS

In order to check the above-mentioned theoretical solutions, an experimental program was performed using a specialized stand, described in detail in [13]. It consists of a 100 mm wide container, with two parallel transparent walls (made of glass), filled with modeling material prepared as a mixture of white cement (50%), bentonite (20%), fine grain sand (10%), coarse grain sand (8%), white vaseline (12%).

All components were heated in a furnace, mixed and cooled to room temperature. Material parameters of this model soil, such as internal friction angle φ and material cohesion c, were measured during a direct shear test and the following values were found: $\varphi = 23.4°$, $c = 19.6\,\mathrm{kPa}$, for unit weight of $\gamma = 18.4\,\mathrm{kN/m^3}$.

In every test, the container was filled with the material layer by layer (20 mm each), and compacted to ensure repeatability of the weight density.

Rigid walls, shaped similarly to those of heavy machine tools, were installed between side walls and fixed, when the medium was moved together with the container at a certain speed V_0. The motion of the material was photographed and later compared with theoretical solutions.

During tests of the cutting process both types of theoretical solutions described in points 3.3.2 and 3.3.3 were experimentally observed. The three slip-lines solution was observed more frequently. This evidence is supported theoretically, since the values of the force which is necessary to realize three slip-lines solution were calculated to be slightly smaller than those for two slip-lines solution. Both theoretical solutions are very close to each other, especially in the advanced stage of cutting, cf. Fig. 12.

In Figs. 13 and 14, two subsequent stages of the cutting process, for the two slip-line cutting mode, are presented. These results can be compared with theoretical solutions shown in Fig. 6 and Fig. 7. An experimentally observed development of the position of the slip line CD (Fig. 5) was marked on the photograph (Fig. 13) by a dotted ($C^{\mathrm{I}}D^{\mathrm{I}}$) and by a dashed line ($C^{\mathrm{III}}D^{\mathrm{III}}$). In Fig. 14, the dotted line was used to indicate the moment of the slip-line CD "jump", when the slip abruptly changes its inclination to a smaller value, after a period of its growth (such a behaviour is described in point 3.3.2 – Fig. 7, line $C^{\mathrm{XI}}H^{\mathrm{I}}$). Since that moment, the cutting mechanism repeats periodically.

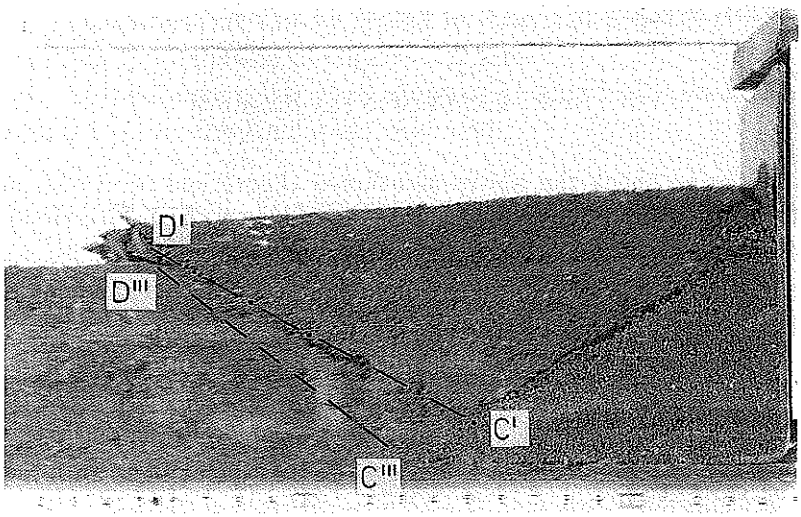

FIG. 13. Two slip-lines cutting mode observed experimentally.

Good correlation between theoretical and experimental results, concerning the slip line CD inclination, change of the inclination angle during the process, and moment of its "jump" is observed. The experimentally measured initial inclination ($\alpha = 60°$) of the slip line $C^{\mathrm{I}}D^{\mathrm{I}}$ coincided, to within the accuracy of 2°, with the theoretically predicted one. In the case of the

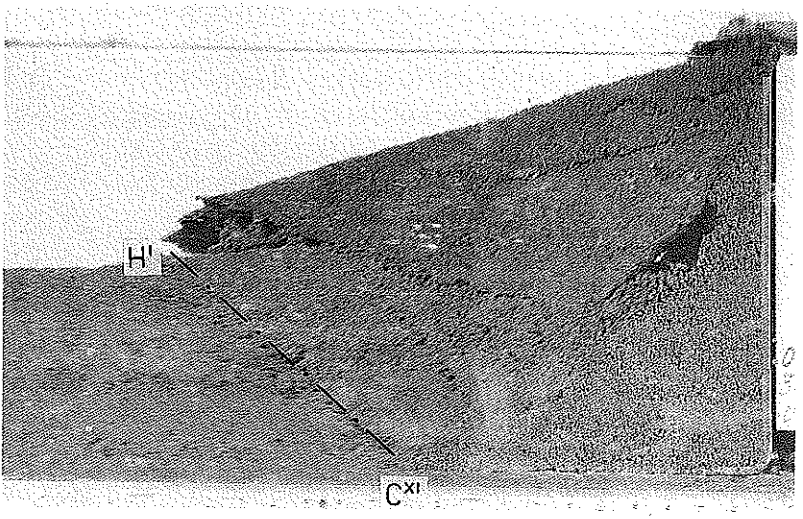

FIG. 14. Advanced stage of the cutting process in the two slip-lines cutting mode (the slip-line "jump") observed experimentally.

slip line $C^{XI}H^{I}$, the experimentally observed inclination ($\alpha = 50°$) and the theoretical prediction coincide even better.

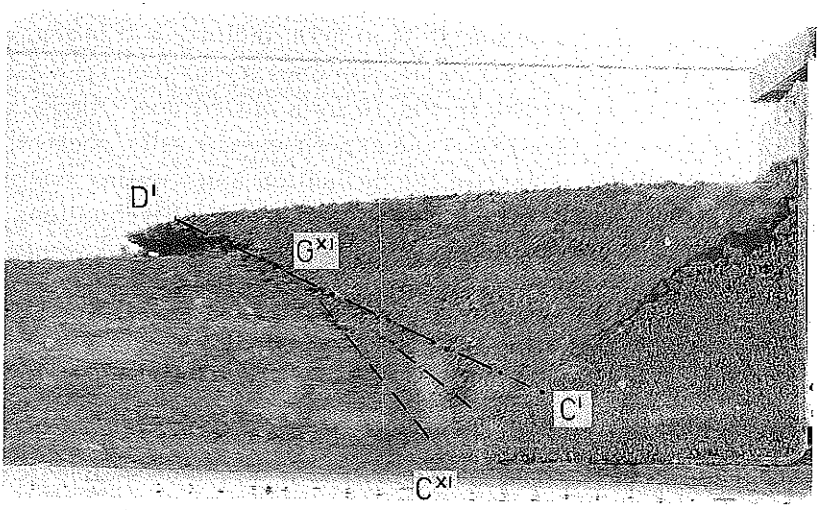

FIG. 15. Three slip-lines cutting mode observed experimentally.

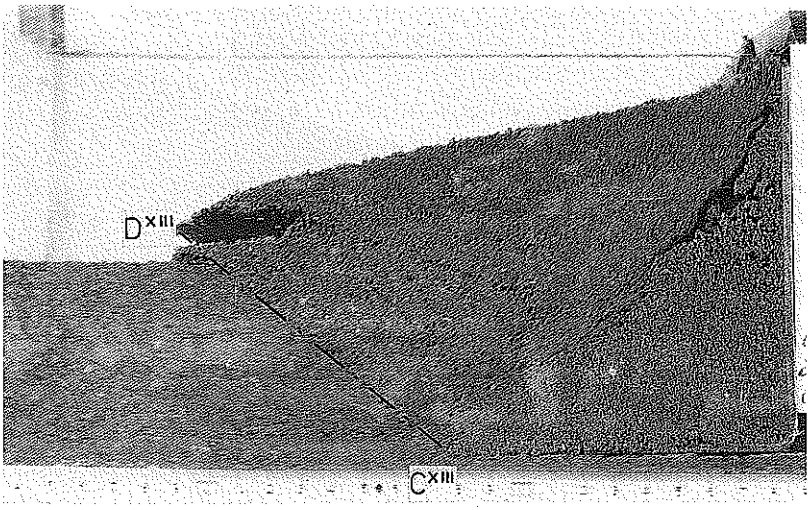

FIG. 16. Advanced stage of the cutting process in the three slip-lines cutting mode (the slip-line "jump") observed experimentally.

Subsequent stages of the cutting process, for the three slip-lines cutting mode, are presented in Fig. 15, 16 (experimental results), for comparison with Figs. 10, 11 (theoretical results). The experimentally observed slip line CG (Fig. 8) and its propagation is marked in the photograph (Fig. 15) by dashed lines. The moment of the slip-line CG abrupt change of inclination to a smaller value, after a period of its growth, indicating transient change from three slip-lines mechanism to two slip-lines mechanism (p. 3.3.3 – line $C^{XIII}D^{XIII}$, Fig. 11), is marked in Fig. 16 by a dotted line. Again, a good correlation between the theoretical and experimental results, concerning the slip line CG inclination, change of the inclination angle during the process, and moment of its "jump" is observed. In the case of inclinations of the $C^{I}D^{I}$ and $C^{XIII}D^{XIII}$ lines, the experimental and theoretical results differ by less than 2 and 1°, respectively.

5. CONCLUSIONS

1. It was shown that, using simple kinematic mechanisms, one can study such complicated processes as those similar to the heavy machine tools working processes. Such solutions cannot be obtained by means of other simplified methods of plasticity.

2. Owing to this simplified approach, characteristic rigid zones generated during the cohesive soil cutting process were predicted, as well as the unstable character of force, which is necessary to realize such a process.

3. For the actually specified shape of the model tool, both cutting modes (two or three slip lines) which were theoretically considered, were observed experimentally. One should remember that the three slip-lines mechanism presented is kinematically inadmissible in the case of the associated flow rule.

4. From the theoretical point of view, the three slip-lines solution is energetically more efficient than the two slip-lines solution. The difference in energy is comparatively small and, because of the material density scatter, the former mechanism can also be observed.

5. The difference between the theoretical and experimental positions of the characteristic slip lines is less than 2°, both for the initial and the advanced stages of the process.

REFERENCES

1. W. SZCZEPIŃSKI, *Some slip-line solutions for earth-moving processes*, AMS, **23**, 6, 1971.
2. W. SZCZEPIŃSKI, *Mechanics of a granular body during the digging process by means of a loading machine* [in Polish], Arch. Bud. Masz., 3, XVIII, 1971.
3. W. SZCZEPIŃSKI, *Limit states and kinematics of granular media* [in Polish], PWN, 1974.
4. V.V. SOKOLOVSKI, *Statics of Soil Media*, 2-nd Ed., Butterworths, London 1960.
5. R.T. SHIELD, *Mixed boundary value problems in soil mechanics*, Q. Appl.Math., **11**, 61, 1953.
6. R.T. SHIELD, *On Coulomb's law of failure in soils*, J. Mech. Phys. Solids, **4**, 10, 1953.
7. W. TRĄMPCZYŃSKI, *The analysis of kinematically admissible solutions for motion of walls of different shape* [in Polish], Theor. Appl. Mechanics, **1**, 15, 1977.
8. R. IZBICKI, Z. MRÓZ, *Plasticity and Limit States*, [in:] *Rock and Soil Mechanics*, W. DERSKI, R. IZBICKI, I. KISIEL and Z. MRÓZ, Elsevier, 1989.
9. J. MACIEJEWSKI, *Incremental analysis of earth-moving mechanisms* [in Polish], (MSc Thesis), Politechnika Warszawska, 1987.
10. W. TRĄMPCZYŃSKI and A. JARZĘBOWSKI, *On the kinematically admissible solution application for theoretical description of shoving processes*, Engng. Trans., **39**, 1, 75–96, 1991.
11. W. TRĄMPCZYŃSKI and J. MACIEJEWSKI, *On the kinematically admissible solutions for soil-tool interaction description in the case of heavy machine working process*, Proc. V-th European Conf. ISTVS, p. 286–303, Hungary, Budapest 1991.

12. R.L. MICHALOWSKI, *Strain localization and periodic fluctuations in granular flow processes from hoppers*, Geotechnique, **40**, 3, 389–403, 1990.

13. D. SZYBA, *Application of simple kinematically admissible solutions to the description of the earth-moving process* [in Polish], PhD Thesis – in preparing.

14. Private discussion with Z. MRÓZ.

15. O. ZIENKIEWICZ, K. LUENG and M. PASTOR, *Simple model for transient soil loading in earthquake analysis. Basic model and its application*, Int. J. Num. Anal. Meth. Geom., **19**, 453–476, 1985.

16. W. SZCZEPIŃSKI and H. WINEK, *Experimental study of granular medium kinetics for certain boundary value problem* [in Polish], Engng. Trans., **20**, 1, 1972.

17. Z. MRÓZ and A. JARZĘBOWSKI, *Phenomenological model of contact slip*, Acta Mech., **102**, 1–4, 59–72, 1994.

POLISH ACADEMY OF SCIENCES
INSTITUTE OF FUNDAMENTAL TECHNOLOGICAL RESEARCH.

Received May 9, 1994; new version October 28, 1994.